Heliyon 10 (2024) e26018

Contents lists available at ScienceDirect

Heliyon

journal homepage: www.cell.com/heliyon

Research article

Dynamics analysis of permanent magnet synchronous motor speed control with enhanced state feedback controller using a linear quadratic regulator

Crescent Onyebuchi Omeje [a], Ayodeji Olalekan Salau [b,d,*], Candidus Ugwoke Eya [c]

[a] Department of Electrical/Electronic Engineering, University of Port Harcourt, Rivers State, Nigeria
[b] Department of Electrical//Electronics and Computer Engineering, Afe Babalola University, Ado-Ekiti, Nigeria
[c] Department of Electrical Engineering, University of Nigeria, Nsukka Enugu State, Nigeria
[d] Saveetha School of Engineering, Saveetha Institute of Medical and Technical Sciences, Chennai, Tamil Nadu, India

ARTICLE INFO

Keywords:
PMSM
Mathematical modeling
Linear quadratic regulator
Disturbance observer
Sliding-mode-observer
PID controller
State-feedback controller
MATLAB-Simulation

ABSTRACT

This paper presents a robust speed regulation and control of a permanent magnet synchronous motor (PMSM). A linear quadratic regulator (LQR) based state feedback controller was developed to achieve a successful suppression of periodic disturbance of speed and torque. Sliding mode observer in conjunction with the disturbance observer was deployed in the control of motor speed. Simulations were carried out based on two compared controllers such as the state feedback controller and the conventional proportional-integral-derivative (PID) controller to attenuate the noisy effects of the external disturbance. A comparative analysis of results showed that a robust as well as an improved speed and torque dynamic performance was achieved with the state feedback (SFC) controller. A reduced periodic disturbance with percentage steady state error values of 24.17% and 23.51% was obtained with the SFC controller as compared to 38.0% and 38.37% obtained using a PID controller. The Eigen values obtained from the derived state feedback matrix (K) based on Ackerman's rule proved that the entire system operation is controllable and the performance index is marginally stable. All simulations were performed using MATLAB/SIMULINK version 2021.

1. Introduction

Technological advancements in automations have shown that PMSM-motors are currently deployed to different electrical and mechanical applications due to their prevailing importance. These include high torque to weight ratio, greater efficiency, simplicity in structure, negligible rotor heating, small moment of inertia and minimized torque ripple [1,2]. The traditional control scheme for PMSM speed is the vector control method which shows that torque angle is kept at $\delta = 90^0$ while ensuring that the reference direct axis current is held at a zero value [3,4]. In recent times, vector control and direct torque regulation in addition to adaptive sliding mode control (ASMC) are the most recommended processes of speed control [5]. In real life applications, applied load disturbances are unavoidable. Hence, establishing a precise steady state speed control with reduced steady state speed error during a distressed state becomes expedient. Externally applied torque is perceived as a major drawback which affects a steady state speed operation of a

* Corresponding author. Department of Electrical//Electronics and Computer Engineering, Afe Babalola University, Ado-Ekiti, Nigeria.
E-mail address: ayodejisalau98@gmail.com (A.O. Salau).

https://doi.org/10.1016/j.heliyon.2024.e26018
Received 3 October 2022; Received in revised form 6 February 2024; Accepted 6 February 2024
Available online 10 February 2024
2405-8440/

Nomenclature

PMSM	Permanent Magnet Synchronous Machine
LQR	Linear Quadratic Regulator
DO	Disturbance Observer
PID	Proportional Integral Derivative Controller
SFC	State Feedback Controller
SMC	Sliding Mode Control
SMO	Sliding Mode Observer
ASMC	Adaptive Sliding Mode Control
ESO	Extended State Observer
T_L	Applied Load Torque
PWM	Pulse Width Modulation
ABCD	State Input and Output Matrix
SMPMSM	Surface Mounted Permanent Magnet Synchronous Machine
αβ	Alpha-beta
$\dot{i}_\alpha$ and $\dot{i}_\beta$	αβ stator currents
$\widehat{\dot{i}}_\alpha$ and $\widehat{\dot{i}}_\beta$	αβ estimated currents
e_α and e_β	αβ Electromotive force
λ_{af}	Rotor flux
ω_r	Electrical angular velocity
ω_{or}	Electrical angular velocity at a quiescent operating state
sgn	Signum function
ω_{mr}	Mechanical angular velocity
ω_{mor}	Mechanical angular velocity at a quiescent operating state
Θ	Theta
ς_b	eta
T_{qdo}	Parks Transformation notation
T_{qdo}^{-1}	Inverse Parks Transformation notation
δ	Load angle also called del
$U_{e(t)}$	State control vector
e(t)	Error vector
$\dot{X}_{(t)}$	Derivative of state variables at time (t)
$\dot{X}_{(\infty)}$	Derivative of state variables at time (∞)
$\omega_r^*(t)$	Electrical angular velocity at time (t)
$\omega_r^*(\infty)$	Electrical angular velocity at time (∞)

permanent magnet synchronous machine (PMSM). The motive of a quality control machine specialist is to regulate or completely reduce the effects of this disturbance on the steady state speed limits. In Refs. [6–8], detailed work on the various forms of disturbance evaluation techniques was discussed. Parameter variations and incorrect adjustment of speed and machine loadability has generated a consequential effect on the steady state speed operation. Presently, emphasis is on how to adopt a pragmatic approach in ensuring that during a transient disturbance, a fast-dynamic response is achieved at a shorter period of time. This reduces the risk of heat dissipation and noisy processes. The contribution and motivation of this paper is to develop a linear quadratic regulator (LQR) based on state feedback controller that minimizes the periodic disturbance in speed and torque. To achieve this process, the Sliding mode observer in conjunction with the disturbance observer was incorporated. Simulations were carried out based on two compared controllers such as the state feedback controller and the conventional proportional-integral-derivative (PID) controller. This was done to illustrate the level of suppression in the periodic disturbance of machine speed and torque as indicated in the frequency spectrum.

2. Related works

Numerous research works have been carried out on PMSM speed control and regulations with the attendant disturbances. In Ref. [9], a problem of stabilization for non-linear delay systems was addressed with exogenous disturbances and event-triggered feedback control. In Ref. [10], output feedback stabilization problem with unknown control coefficients and output function was reported. Disturbance estimation was examined on PMSM speed controller using extended state observer (ESO) and was presented in Refs. [11,12]. Parameter variation with mismatched uncertainty for non-linear disturbance observer control was applied in the PMSM drive system as reported in Ref. [13]. In Ref. [14], a predictive control with extended state observer was used in optimizing the PMSM control performance while in Ref. [15], a reference model adaptive control with estimated disturbance was applied in speed regulation for a constrained state feedback. In Ref. [16], an extreme sliding mode speed regulation method was presented. In Ref. [17], a

Sensorless PMSM speed control with disturbance and observer method was realized. In Ref. [18], a composite speed controller for PMSM was developed in an uneven disturbance. Fractional order proportional integral controller was developed for the control of the PMSM speed [19]. Controllers with dual degree of freedom were adopted for robust speed control. A model predictive speed control applied in speed ripple minimization of the PMSM was detailed in Ref. [20]. A novel approach of PMSM speed control with anti-disturbance sliding mode was also reported in Ref. [21].

A current control with disturbance observer for PMSM speed drives using an adaptive sliding mode was presented in Ref. [22]. A speed controller design was proposed for PMSM drives using only SMC and was presented in Ref. [23]. Zhang et al. [24] also presented a non-linear PMSM speed control with sliding mode and disturbance compensation. Combination of PMSM speed with current for terminal sliding mode control and non-linear disturbance observers was illustrated in Ref. [25]. Authors in Ref. [26] presented an SMC with a non-linear fractional order PID sliding surface for the speed performance of surface mounted PMSM drives based on an extended state observer. Authors in Ref. [27] described a work on PMSM servo-drive control system with state feedback and load torque using feed forward compensation. In Ref. [28], a simplified two degrees of freedom for robust speed control of PMSM was reported. It is worthy of note that in all the literature reviewed material, speed control was accomplished with the aid of different controller's design which gave different percentage steady state error value under negative perturbation. New method applied here involved a close monitoring of the disturbance in order to readjust the speed operational point which constantly is updated with disturbance-observer method during speed perturbation. A state feedback controller (SFC) was designed using the updated linearized model obtained from a linear-quadratic regulator. In addition, an optimal control index was obtained using Ackerman's method and a comparison was drawn from simulation results on cascaded operations based on improved sliding mode with disturbance-observer and a PID-controller's approach. This work is organised as follows: Section 1 presents the introduction, while section 2 presents the reviewed literature. Section 3 presents the research methodology and discusses the PMSM mathematical modeling in non-linear and linear states with the design of an optimal linear quadratic regulator algorithm. Section 4 presents the results of simulation. Section 5 presents the conclusion and recommendation.

3. Methodology

3.1. PMSM mathematical modeling and design of optimal linear quadratic regulator

The voltage equation of each stator winding for a PMSM is usually the summation of the resistive voltage drop and the voltage induced from the time varying flux linkage. The three phase voltage equation is therefore presented in Eq. (1).

$$\left.\begin{aligned} V_a &= r_a i_a + \frac{d\lambda_a}{dt} \\ V_b &= r_b i_b + \frac{d\lambda_b}{dt} \\ V_c &= r_c i_c + \frac{d\lambda_c}{dt} \end{aligned}\right\} \tag{1}$$

The stator windings are wound with the same number of turns so that their separate resistance is equal in all the three windings with $r_a = r_b = r_c = r_s$. In matrix form, the modified voltage equation is represented in Eq. (2).

$$V_{abc} = R_s i_{abc} + \frac{d\lambda_{abc}}{dt} = \begin{bmatrix} r_s & 0 & 0 \\ 0 & r_s & 0 \\ 0 & 0 & r_s \end{bmatrix} \times \begin{bmatrix} i_a \\ i_b \\ i_c \end{bmatrix} + \frac{d}{dt}\begin{bmatrix} \lambda_a \\ \lambda_b \\ \lambda_c \end{bmatrix} \tag{2}$$

To transform the three phase PMSM voltage equation from abc to dqo, the Park transformation technique was applied as presented in Eq. (3).

$$\begin{bmatrix} S_q \\ S_d \\ S_o \end{bmatrix} = T_{qdo} \times \begin{bmatrix} S_a \\ S_b \\ S_c \end{bmatrix} \tag{3}$$

where: S represents voltage, current and power in their respective domains. Also q, d and o are the quadrature, direct and zero sequence variables. The transformation factor T_{qdo} and its inverse are obtained from Eqs. (4) and (5).

$$T_{qdo} = \frac{2}{3} \times \begin{bmatrix} \cos\theta & \cos\left(\theta - \frac{2\pi}{3}\right) & \cos\left(\theta + \frac{2\pi}{3}\right) \\ \sin\theta & \sin\left(\theta - \frac{2\pi}{3}\right) & \sin\left(\theta + \frac{2\pi}{3}\right) \\ \frac{1}{2} & \frac{1}{2} & \frac{1}{2} \end{bmatrix} \tag{4}$$

$$T_{qdo}^{-1} = \begin{bmatrix} \cos\theta & \sin\theta & 1 \\ \cos\left(\theta - \frac{2\pi}{3}\right) & \sin\left(\theta - \frac{2\pi}{3}\right) & 1 \\ \cos\left(\theta + \frac{2\pi}{3}\right) & \sin\left(\theta + \frac{2\pi}{3}\right) & 1 \end{bmatrix} \tag{5}$$

Ideally, motors are operated with the neutral point floating since current is not allowed to flow in the neutral. Therefore, the zero sequence is usually not considered in the actual analysis of the machine. Expressing V_{abc} into V_{qdo} variable gives rise to Eq. (6). Further transformation of Eq. (6) gives rise to Eq. (7).

$$V_{abc} = R_s i_{abc} + \frac{d\lambda_{abc}}{dt} = R_s T_{qdo}^{-1} i_{qdo} + \frac{d}{dt}\left(T_{qdo}^{-1} \lambda_{qdo}\right) \tag{6}$$

$$V_{qdo} = T_{qdo} R_s T_{qdo}^{-1} i_{qdo} + T_{qdo}\frac{d}{dt}\left(T_{qdo}^{-1}\lambda_{qdo}\right) \tag{7}$$

The detailed simplification of Eq. (7) as cited in Ref. [29] is presented in Eq. (8)

$$V_{qdo} = R_s i_{qdo} + \omega_r \times \begin{bmatrix} \lambda_d \\ -\lambda_q \\ 0 \end{bmatrix} + \frac{d\lambda_{qdo}}{dt} \tag{8}$$

The mathematical modeling of the PMSM is developed based on Eq. (8) and also on the vector control where the axis of rotor rotating flux aligns with the d-axis of the machine. It is presumed that the inductance is independent of the rotor position. The basic non-linear models for electrical and mechanical equations of surface mounted permanent magnet synchronous machine equations are given in Eqs. (9-12) as referenced in Ref. [30].

$$V_q = R_s i_q + L\frac{di_q}{dt} + \omega_r L i_d + \omega_r \lambda_{af} \tag{9}$$

$$V_d = R_s i_d + L\frac{di_d}{dt} - \omega_r L i_q \tag{10}$$

$$\frac{d\omega_{mr}}{dt} = \frac{1}{J}\left(T_e - T_L - B\omega_{mr}\right) \tag{11}$$

$$T_e = \frac{3}{2} \times \frac{P}{2} \times i_q \times \left(\lambda_{af}\right) \tag{12}$$

In state space, Eqs. (9-12) can be re-arranged to Eqs. (13-15).

$$\frac{di_q}{dt} = \frac{V_q}{L} - \frac{R_s}{L} i_q - \omega_r i_d - \frac{\lambda_{af}}{L}\omega_r \tag{13}$$

$$\frac{di_d}{dt} = \frac{V_d}{L} - \frac{R_s}{L} i_d + \omega_r i_q \tag{14}$$

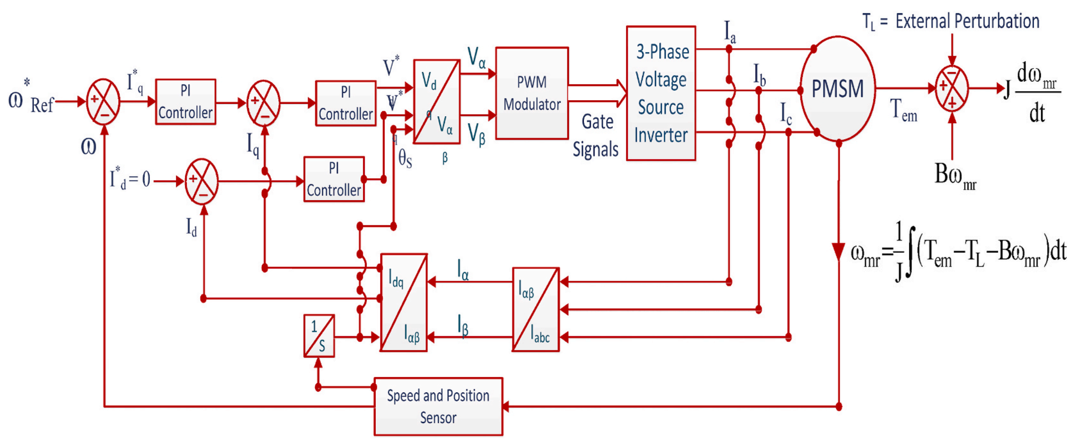

Fig. 1. Conventional closed-loop control diagram of the PMSM with speed sensor.

$$\frac{d\omega_{mr}}{dt} = \frac{K_t}{J} i_q - \frac{B}{J}\omega_{mr} - \frac{P}{2 \times J} T_L \tag{15}$$

The mechanical and the electrical speed are related by Eq. (16).

$$\omega_r = \frac{P}{2}\omega_{mr} \tag{16}$$

where: $[i_q \quad i_d \quad \omega_{mr}]$ are system states, $[V_q \quad V_d]$ represents inputs of the system. The external disturbance which is given by Eq. (17) is dependent on the applied load torque T_L.

$$d = -\frac{P}{2J} T_L \tag{17}$$

where: J = moment of inertia of the mechanical axis (kgm^2), T_L = applied load torque (Nm), ω_{mr} = mechanical speed of the machine (Rad/Sec), B = coefficient of viscous friction (Nms^2).

Fig. 1 illustrates the conventional closed loop outline for permanent magnet synchronous motor (PMSM) drive.

A Jacobian linearization method for Eqs. (13-16) is presented in Eq. (18) for a linearized function [30].

$$\dot{X} = \begin{bmatrix} \frac{-R_s}{L} & -\omega_{or} & \frac{-(\lambda_{af} + LI_{do})}{L} \\ \omega_{or} & \frac{-R_s}{L} & i_{qo} \\ \frac{K_t}{J} & 0 & \frac{-B}{J} \end{bmatrix} + \begin{bmatrix} \frac{1}{L} & 0 \\ 0 & \frac{1}{L} \\ 0 & 0 \end{bmatrix} u + \begin{bmatrix} 0 \\ 0 \\ 1 \end{bmatrix} d \tag{18}$$

The model presented in Eq. (18) is a PMSM linearized model around an operating point $[i_{qo} \quad i_{do} \quad \omega_{or}]$. For a vector control, a constant torque angle of $\delta = 90^0$ is required which gives rise to $i_d = 0$ while $i_{qo} = i_q^*$ which varies as the load torque changes. In steady state condition, the load torque is always equivalent to the motor developed torque given by Eq. (19).

$$T_L = T_e \tag{19}$$

Substituting Eq. (12) into Eq. (19) while observing the vector control conditions gives rise to Eq. (20).

$$i_q^* = i_{qo} = \frac{T_L}{\left(\frac{3}{2} \frac{P}{2} \lambda_{af}\right)} \tag{20}$$

Based on Eq. (20), it is obvious that i_{qo} is dependent on the disturbance and is refreshed using a disturbance-observer (DO) with a new operating point $[i_{qo} \quad i_{do} \quad \omega_{mor}]$ successfully updated. Two cascade observers which include sliding mode observer and disturbance observer are used for speed estimation and disturbance. Sliding mode is a generally known technique applied in hardware implementation [25,26,31–33]. Sliding mode observer is achieved using PMSM equation model based on Clark's αβ coordinate transformation system. Therefore, transforming Eqs. (9) and (10) into αβ coordinate with the back emf incorporated gives rise to Eqs. (21) – (24).

$$L\frac{di_\alpha}{dt} = -Ri_\alpha - e_\alpha + V_\alpha \tag{21}$$

$$L\frac{di_\beta}{dt} = -Ri_\beta - e_\beta + V_\beta \tag{22}$$

$$e_\alpha = -\lambda_{af}\,\omega_r \sin\theta \tag{23}$$

$$e_\beta = -\lambda_{af}\,\omega_r \cos\theta \tag{24}$$

The surface current chosen are presented in Eqs. (25–27).

$$S = \hat{\dot{i}}_s - \dot{i}_s \tag{25}$$

$$\dot{i}_s = [\dot{i}_\alpha \quad \dot{i}_\beta] \tag{26}$$

$$\hat{\dot{i}}_s = [\hat{\dot{i}}_\alpha \quad \hat{\dot{i}}_\beta] \tag{27}$$

where: $\dot{i}_\alpha$ and $\dot{i}_\beta$ are αβ stator currents, $\hat{\dot{i}}_\alpha$ and $\hat{\dot{i}}_\beta$ are αβ estimated currents, e_α and e_β are the αβ Electromotive force, λ_{af} is the rotor flux, ω_r is electrical angular velocity (Rad/Sec.). On attaining sliding surface, S is zero while $\hat{\dot{i}}_\alpha = \dot{i}_\alpha$ and $\hat{\dot{i}}_\beta = \dot{i}_\beta$. The observer is therefore robust under this condition. The back emf also changes with the new expression obtained based on the dynamic equations presented in

Eqs. (28) and (29).

$$L\frac{d\hat{i}_\alpha}{dt} = -R\hat{i}_\alpha - K_x \operatorname{sgn}(\hat{i}_\alpha - i_\alpha) + V_\alpha \tag{28}$$

$$L\frac{d\hat{i}_\beta}{dt} = -R\hat{i}_\beta - K_x \operatorname{sgn}(\hat{i}_\beta - i_\beta) + V_\beta \tag{29}$$

Comparing Eqs. (21) and (22) with Eqs. (28) and (29) gives rise to the emf equation given in Eq. (30).

$$\left.\begin{aligned} \hat{e}_\alpha &= K_x \operatorname{sgn}(\hat{i}_\alpha - i_\alpha) \\ \hat{e}_\beta &= K_x \operatorname{sgn}(\hat{i}_\beta - i_\beta) \end{aligned}\right\} \tag{30}$$

As earlier mentioned, the externally applied load torque is considered as a disturbance. This disturbance is assessed with a disturbance-observer equation presented in Eq. (31).

$$\frac{d\omega_{mr}}{dt} = \frac{1}{J}\left(\frac{3}{2}\,\frac{P}{2}\lambda_{af}\, i_q - T_L - B\omega_{mr}\right) \tag{31}$$

Selecting state variables as $x = \omega_{mr}$, disturbance as $d = \frac{-T_L}{J}$, $K_T = \frac{1}{J}\,\frac{3}{2}\,\frac{P}{2}\,\lambda_{af}$. Then Eq. (31) gives rise to Eq. (32).

$$\dot{X} = \frac{-B}{J}X + K_T i_q + d \tag{32}$$

The disturbance is presumed as a gradually changing load torque disturbance which can be compensated with a properly designed controller. A controller is designed based on the linearized model presented in Eq. (18) which is compactly denoted in Eq. (33).

$$\left.\begin{aligned} \dot{X} &= Ax + B_u U + B_d d \\ Y &= Cx \end{aligned}\right\} \tag{33}$$

$A = \begin{bmatrix} \frac{-R_s}{L} & -\omega_{or} & \frac{-(\lambda_{af} + LI_{do})}{L} \\ \omega_{or} & \frac{-R_s}{L} & i_{qo} \\ \frac{K_t}{J} & 0 & \frac{-B}{J} \end{bmatrix}$; $B_u = \begin{bmatrix} \frac{1}{L} & 0 \\ 0 & \frac{1}{L} \\ 0 & 0 \end{bmatrix}$; $B_d = \begin{bmatrix} 0 \\ 0 \\ 1 \end{bmatrix}$; $C = [\,0\ \ 0\ 1\,]$; $x = [\,i_q\ i_d\ \omega_r\,]^T$; $U = [V_q\ V_d]^T$. The initial steady-state operating point is given by $x_o = [\,i_{qo}\ i_{do}\ \omega_{or}\,]$

A linear state feedback controller (SFC) meant for tracking the anticipated result is gotten from a Linear-Quadratic Regulator (LQR) [16,34,35]. A modified block diagram of Fig. 1 with SMO and DO incorporated is presented in Fig. 2 as the Sensorless based vector control model.

A linear quadratic regulator is an optimal control problem where machine state equation is made linear, the cost function is quadratic and the test conditions comprise the initial condition on the state with no disturbance input. A conventional state feed controller (SFC) is always designed using state errors. For a design with negligible steady state error in speed, an integral feedback controller is applied as presented in Eq. (34).

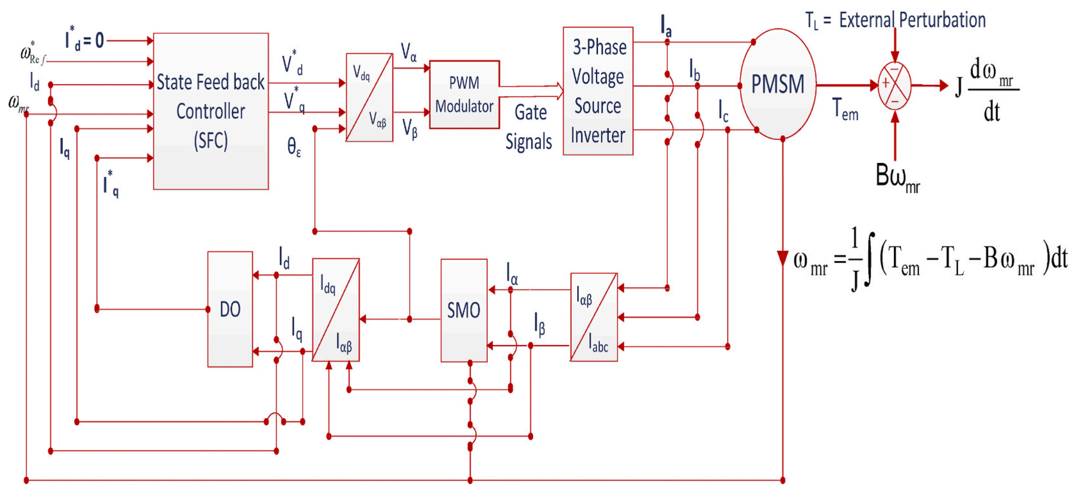

Fig. 2. Modified block diagram of the Sensorless PMSM vector control with SMO and DO.

$$U = -K_x\,(X^* - X) + K_b\varsigma_b \tag{34}$$

Where: $\varsigma_b = (\omega_r^* - \omega_{or})$. Augmenting Eqs. (33) and (34) gives rise to Eq. (35).

$$\begin{bmatrix}\dot{X}_{(t)}\\ \dot{\varsigma}_{b(t)}\end{bmatrix} = \begin{bmatrix}A & 0\\ -C & 0\end{bmatrix}\begin{bmatrix}x_{(t)}\\ \varsigma_{b(t)}\end{bmatrix} + \begin{bmatrix}B\\ 0\end{bmatrix}U(t) + \begin{bmatrix}B_d\\ 0\end{bmatrix}d(t) + \begin{bmatrix}B\\ 0\end{bmatrix}\omega_r^*(t) \tag{35}$$

When $t = \infty$, Eq. (35) changes to Eq. (36) as presented.

$$\begin{bmatrix}\dot{X}_{(\infty)}\\ \dot{\varsigma}_{b(\infty)}\end{bmatrix} = \begin{bmatrix}A & 0\\ -C & 0\end{bmatrix}\begin{bmatrix}x_{(\infty)}\\ \varsigma_{b(\infty)}\end{bmatrix} + \begin{bmatrix}B\\ 0\end{bmatrix}U(\infty) + \begin{bmatrix}B_d\\ 0\end{bmatrix}d(\infty) + \begin{bmatrix}B\\ 0\end{bmatrix}\omega_r^*(\infty) \tag{36}$$

Subtracting Eq. (36) from Eq. (35) gives rise to Eq. (37).

$$\begin{bmatrix}\dot{X}_{(t)} - \dot{X}_{(\infty)}\\ \dot{\varsigma}_{b(t)} - \dot{\varsigma}_{b(\infty)}\end{bmatrix} = \begin{bmatrix}A & 0\\ -C & 0\end{bmatrix}\begin{bmatrix}x_{(t)} - x_{(\infty)}\\ \varsigma_{b(t)} - \varsigma_{b(\infty)}\end{bmatrix} + \begin{bmatrix}B\\ 0\end{bmatrix}U_{(t)} - U_{(\infty)} + \begin{bmatrix}B_d\\ 0\end{bmatrix}d_{(t)} - d_{(\infty)} +$$

$$\begin{bmatrix}B\\ 0\end{bmatrix}\omega_{r(t)}^{*} - \omega_{or(\infty)}^{*} \tag{37}$$

In a compact arrangement, Eq. (37) can be rewritten as presented in Eq. (38).

$$\begin{bmatrix}\dot{X}_{e(t)}\\ \dot{\varsigma}_{e(t)}\end{bmatrix} = \begin{bmatrix}A & 0\\ -C & 0\end{bmatrix}\begin{bmatrix}x_{e(t)}\\ \varsigma_{e(t)}\end{bmatrix} + \begin{bmatrix}B\\ 0\end{bmatrix}U_{e(t)} + \begin{bmatrix}B_d\\ 0\end{bmatrix}d_{e(t)} + \begin{bmatrix}B\\ 0\end{bmatrix}\omega_{e(t)}^{*} \tag{38}$$

where: $\dot{X}_{e(t)} = \dot{X}_{(t)} - \dot{X}_{(\infty)}$; $\dot{\varsigma}_{e(t)} = \dot{\varsigma}_{b(t)} - \dot{\varsigma}_{b(\infty)}$; $x_{e(t)} = x_{(t)} - x_{(\infty)}$; $\varsigma_{e(t)} = \varsigma_{b(t)} - \varsigma_{b(\infty)}$; $U_{e(t)} = U_{(t)} - U_{(\infty)}$; $d_{e(t)} = d_{(t)} - d_{(\infty)}$; $\omega_{e(t)}^{*} = \omega_{(t)}^{*} - \omega_{(\infty)}^{*}$.

A relational equation for the control vector $U_{e(t)}$ and the error vector $e(t)$ is defined by Eq. (39).

$$\dot{e}(t) = \widehat{A}e(t) + \widehat{B}Ue(t) \tag{39}$$

where: $\widehat{A} = \begin{bmatrix}A & 0\\ -C & 0\end{bmatrix}$; $\widehat{B} = \begin{bmatrix}B\\ 0\end{bmatrix}$; $Ue(t) = -Ke(t)$; $K = \begin{bmatrix}k_x\\ k_b\end{bmatrix}^T$. The simplified state equation that represents the error vector with the system matrix is presented in Eq. (40).

$$\dot{e}(t) = (\widehat{A} - \widehat{B}K)e \tag{40}$$

So, by direct placement of the Eigen vector in Eq. (40) and by verifying the resultant values through MATLAB, the nature of the stability error $e(t)$ limit is obtained. A linear quadratic regulator generally is intended to curtail a quadratic performance measure of a non-linear equation. A reliable cost function to use when the control system is designed to operate for a long period of time is given by Eq. (41).

$$J = \frac{1}{2}\int\left(x_{(t)}^T\,Q\,x_{(t)} + U_{(t)}^T R U_{(t)}\right)\,dt \tag{41}$$

Table 1
Simulation parameters used.

Parameters	Values
Inverter Carrier Frequency (kHz)	5
Modulation index	0.8
PMSM rated power (hP)	15
Supply Frequency (Hz)	50
Rated phase voltage (V)	220
Stator resistance (Ω)	0.875
Inductance (mH)	8.75
Flux linkage (Weber-Turn)	0.0175
d-axis operating current (A)	2
Moment of Inertia (kgm^2)	0.0875
Viscous friction (N.M.S)	0.00003075
Number of Poles	8
Load torque (Nm)	0.85
Synchronous speed (Rad./Sec.)	78.55
Proportional Controller	1.25
Integral Controller	0.025
Derivative Controller	0.000025

In this case, $Q \geq 0$ and $R > 0$ though their values are determined by control Engineer or designers. In this work, Q and R values are chosen as unity matrix for accuracy and simplicity.

$Q = [100,010,001]$ and $R = 1$. The state feedback matrix gain (K) is shown in Eq. (42). Where P is the solution to the algebraic matrix Riccati equation as presented in Eq. (43).

$$K = R^{-1} B^T P x_{(t)}^T \tag{42}$$

$$PA + A^T P - PBR^{-1} B^T P + Q = 0 \tag{43}$$

The most commonly used approach in determining the value of (P) is built on trial-and-error method. Therefore, substituting the value of the machine parameter in Table 1 into the state system matrix gives rise to a solution of Eq. (43).

$$PA = \begin{bmatrix} P_{11} & P_{12} & P_{13} \\ P_{12} & P_{22} & P_{23} \\ P_{13} & P_{23} & P_{33} \end{bmatrix} \begin{bmatrix} -100 & -314.2 & -4 \\ 314.2 & -100 & 2 \\ 152.8 & 0 & 0 \end{bmatrix} A^T P = \begin{bmatrix} -100 & 314.2 & 152.8 \\ -314.2 & -100 & 0 \\ -4 & 2 & 0 \end{bmatrix} \begin{bmatrix} P_{11} & P_{12} & P_{13} \\ P_{12} & P_{22} & P_{23} \\ P_{13} & P_{23} & P_{33} \end{bmatrix}.$$

$P_{12} = P_{21}$, $P_{23} = P_{32}$, $P_{13} = P_{31}$, $B = [001]$ and $B^T = [0\ 0\ 1]$.

The SFC gain K in Eq. (42) can be calculated by substituting these matrix variables into the Riccati equation in Eq. (43) to solve for P-values but this may result to a complex matrix computation with attendant error. Therefore, a simplified LQR algorithm which minimizes the performance index is presented in Fig. 3 which evaluates the SFC gain K with high accuracy that is in conformity with [36].

4. Results and discussion

Table 1 contains the simulation parameters applied in this work. In Fig. 4, dq-axes currents of the PMSM with state feedback controller were presented while Fig. 5 contains dq-axes current with PID controller. It is obvious in both Figures that the transient response time with the PID controller during an external disturbance was more pronounced than with the SFC controller. This could result in an undesirable noise and vibration in the PMSM. In Figs. 6 and 7, rotor speed with SFC controller and PID controller were presented. It is observed that the speed response with the SFC controller on full load is very much improved and has a lower percentage steady state error of 24.17% due to reduced settling time of 0.725817 Sec. A synchronous speed of 78.544 Rad/Sec. was also attained at a faster rate with the SFC controller during a full load operation. The speed response to an external disturbance using the PID controller showed that more ripples were obtained which took a longer duration of 1.13997 Sec. before attaining a steady state condition. This also gave rise to a higher percentage steady state error value of 38.0%. Table 2 showed that an improved dynamic performance was achieved with the SFC controller. In Figs. 8 and 9, the electromagnetic torque ripples were reduced using the SFC controller whereas with a PID-controller, an undesirably high oscillation was obtained. The percentage steady state error is expressed as: $\frac{\text{Settling Time (Sec.)}}{\text{Simulation Time (Sec.)}} \times 100\%$. Therefore in Table 2, the percentage steady state error in torque indicated that 38.37% was produced with a PID-controller as opposed to 23.51% produced with SFC controller. In Figs. 10 and 11, the power outputs of the two controllers were

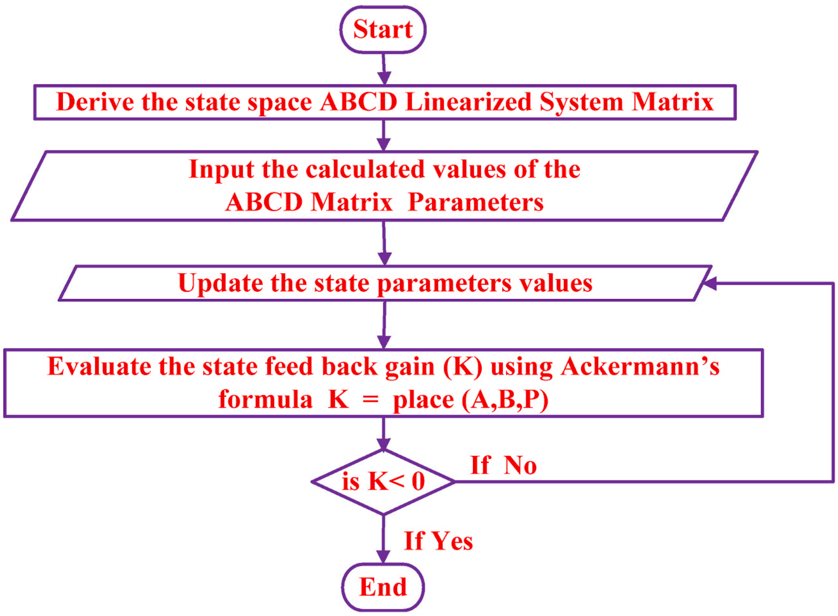

Fig. 3. State Feedback gain (K) algorithm with LQR.

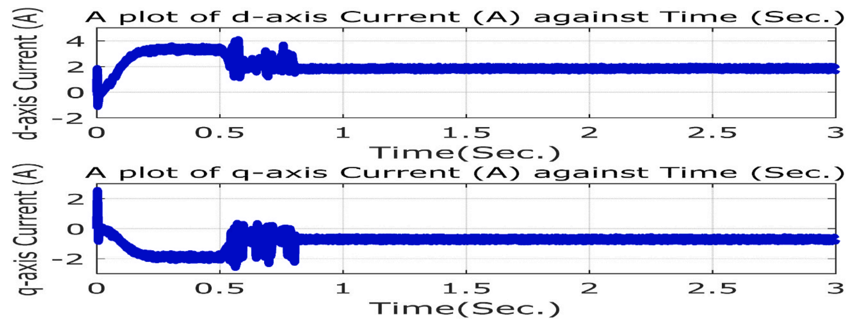

Fig. 4. dq-axes Current with SFC-Controller.

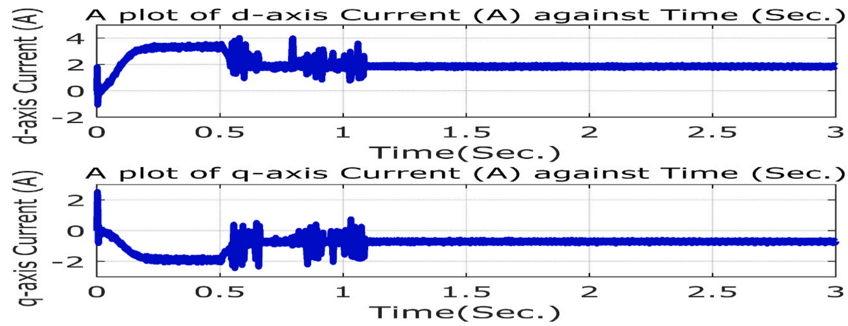

Fig. 5. dq-axes Current with PID-Controller.

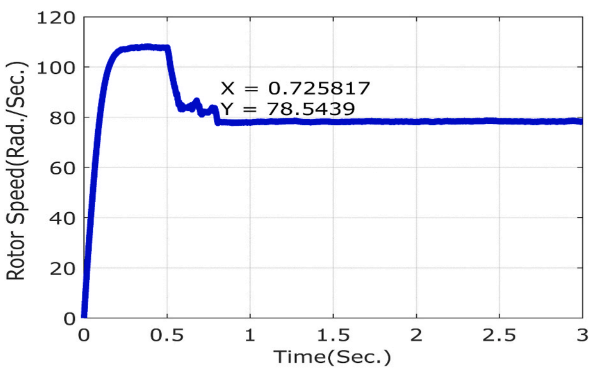

Fig. 6. Rotor speed (Rad/Sec.) with SFC-controller.

presented. It is also observed that the steady state power output with SFC controller was attained at a faster rate with a settling time of 0.82017 Sec. and with a reduced percentage error value of 27.35% as against 38.84% obtained using a PID controller. In Figs. 12 and 13, it is observed that torque-speed characteristics with SFC controller prior to the attainment of synchronous speed value of 78.55 Rad/Sec. exhibited a slight transient characteristic which is less severe as compared with the PID controller. The inverter phase A gate signal is presented in Fig. 14. It is shown in this Fig. 14 that IGBT2-Gate signal is complementary to IGBT1-Gate signal and therefore cannot be turned on simultaneously. The inverter phase voltage and current are shown in Fig. 15. A close observation showed that the current is almost in phase with the voltage which is indicative of a unity power factor operation. The frequency spectrums for the speed and torque dynamics are presented in Figs. 16 and 17. The plots indicated that the SFC enabled a robust and extremely high attenuation of periodic disturbances in the PMSM drive system. It can be observed that the spectrum with a PID controller contained several harmonic components which gave rise to acoustic noise and machine overheating during fluctuating load operation.

In Fig. 18, it is observed that the Sensorless control system performed well during the start-up operation as shown in the actual speed of the machine, while the estimated speed took a longer duration before attaining a steady state and also tracked the actual speed after 0.5 Sec. A drop in speed was observed during a load change of 0.85Nm which was restored to a steady state synchronous speed of 78.57 Rad/Sec at 1.403 Sec. In Fig. 19, the start-up transient in the actual torque developed by the machine was very minimal as compared to the estimated torque. The steady state attainment was achieved at a faster rate as seen in the actual developed torque

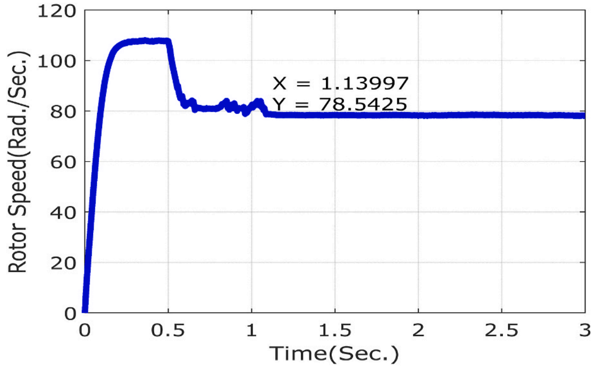

Fig. 7. Rotor speed (Rad/Sec.) with PID-Controller.

Table 2
Performance characteristics of the PMSM based on simulation results.

Varying Parameters	Settling Time (Sec.)	Simulation Time (Sec.)	Steady State error (%) $\frac{\text{Settling Time (Sec.)}}{\text{Simulation Time (Sec.)}} \times 100$
Speed with PID Controller	1.13997	3	38.00
Speed with SFC Controller	0.725817	3	25.09
Electromagnetic Torque with PID Controller	1.15108	3	38.37
Electromagnetic Torque with SFC Controller	0.70508	3	23.51
Power output with PID Controller	1.16536	3	38.84
Power output with SFC Controller	0.820417	3	27.35

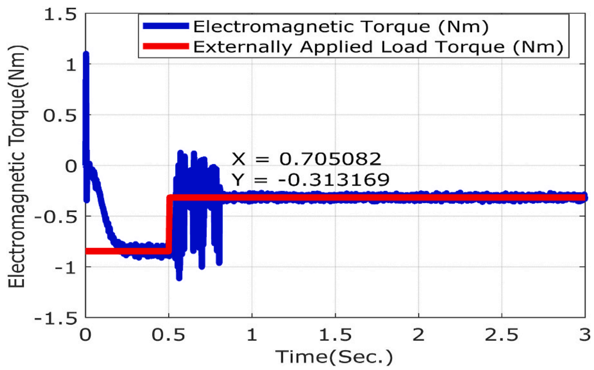

Fig. 8. Torque (Nm.) with SFC-controller.

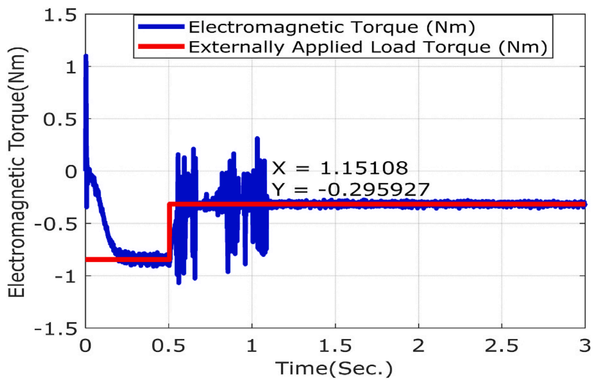

Fig. 9. Torque (Nm.) with PID-Controller.

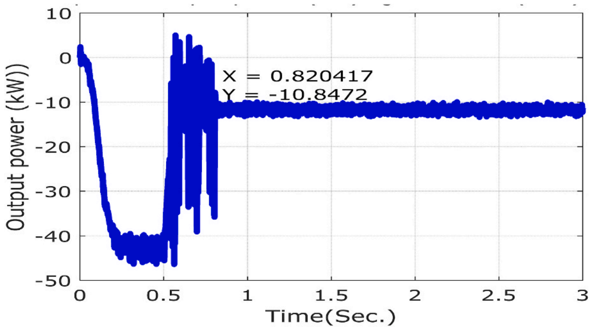

Fig. 10. Output power (kW) with SFC-Controller.

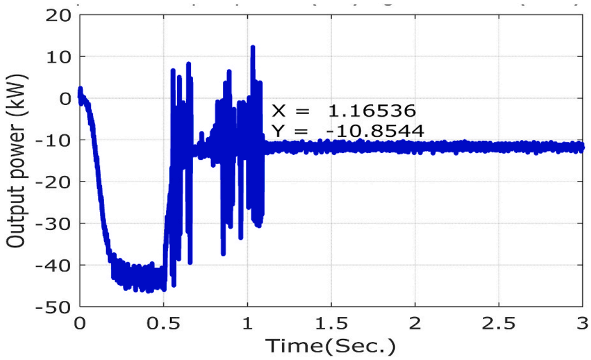

Fig. 11. Output power (kW) with PID-Controller.

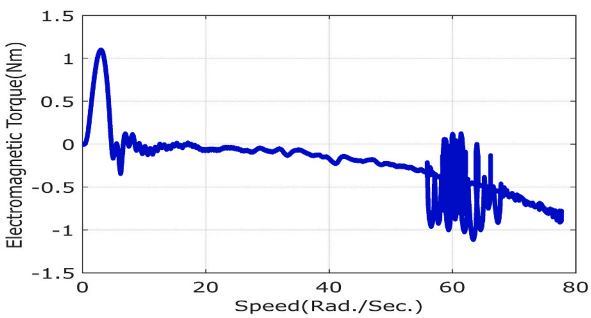

Fig. 12. Torque against speed with SFC-controller.

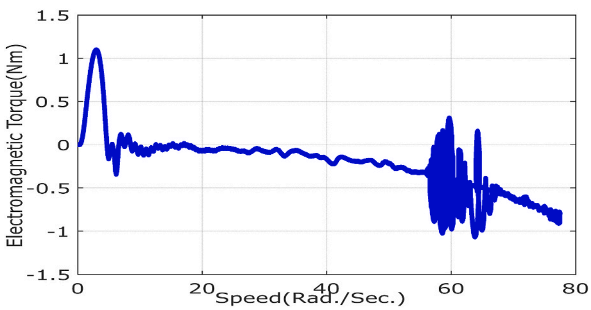

Fig. 13. Torque against speed with PID-Controller.

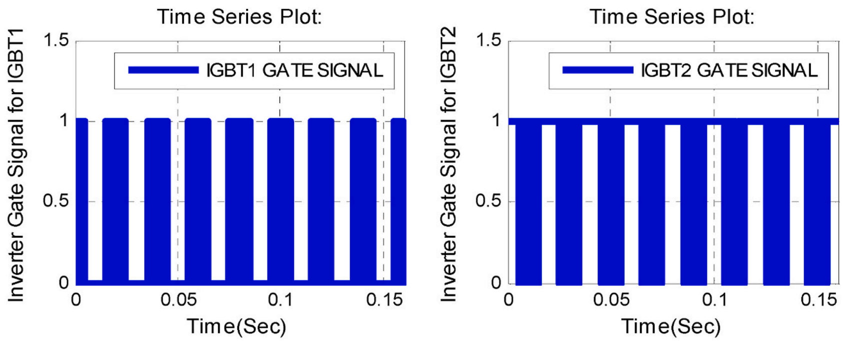

Fig. 14. Phase A inverter gate signals.

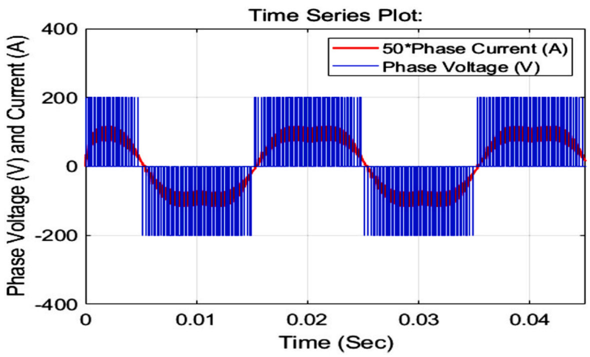

Fig. 15. Inverter phase voltage (V) and current (A).

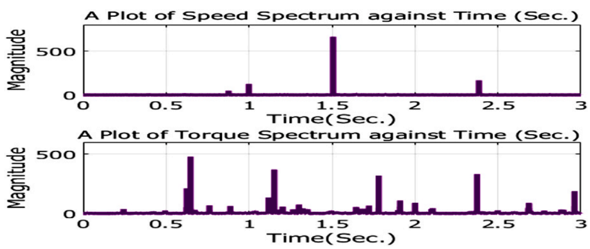

Fig. 16. Plot of speed and torque spectrum against time (Sec.) with SFC-controller.

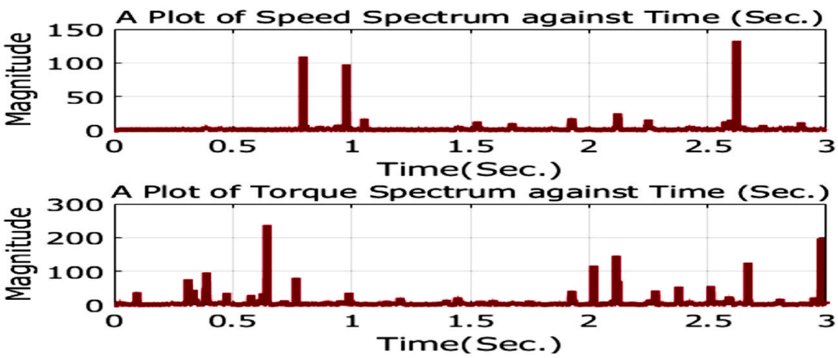

Fig. 17. Plot of speed and torque spectrum against time (Sec.) with PID-Controller.

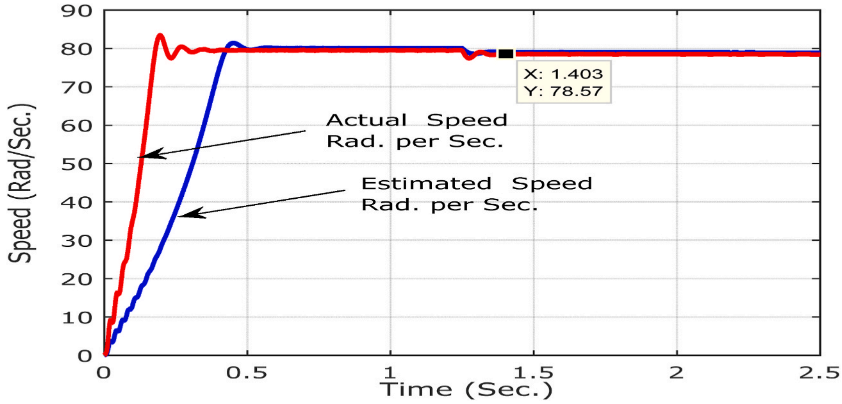

Fig. 18. Speed response to Load Changes for a Sensorless PMSM Drive Control.

waveform before it closely tracked the estimated torque. A rise in torque was also observed at 1.327 Sec. before a steady state condition was regained. The dq-axes current for the vector controlled Sensorless speed controlled PMSM is presented in Fig. 20. It is observed that the d-axis current is completely zero for vector controlled operation while the q-axis current oscillated between 20 A and −20 A at 0.5 Sec. The Eigen value obtained from the algorithm earlier presented in Fig. 3 using the state feedback matrix showed that the system equation is controllable with the following values: $\lambda_1 = -99.698 + j315.08$, $\lambda_2 = -99.698 - j315.08$, and $\lambda_3 = -0.6036$. The state feedback gain obtained based on the algorithm presented in Fig. 3 is given by $K = \begin{bmatrix} 0.0870 & -0.2749 & 0.6219 \\ 0.2749 & -0.0870 & 0.0001 \end{bmatrix} \begin{bmatrix} X_1 \\ X_2 \\ X_3 \end{bmatrix}$. The performance control index is therefore minimized by $K = \begin{bmatrix} 0.0870X_1 & -0.2749X_2 & 0.6219X_3 \\ 0.2749X_1 & -0.0870X_2 & 0.0001X_3 \end{bmatrix}$.

5. Conclusion and recommendations

5.1. Conclusion

In this paper, a non-linear PMSM modeled equation was derived and linearized, while a state feedback controller design based on the linearized model was achieved with a linear quadratic regulator (LQR). The state feedback matrix K derived from Ackerman's technique with the computed Eigen values shows that the entire system is controllable and the performance index is marginally stable. The displayed simulation results indicate that a substantial enhancement in machine dynamic performance was achieved using the state feedback controller as manifested in the reduced percentage steady state error obtained from the motor speed, electromagnetic torque and power output. The frequency spectrum also indicates that a robust and an extremely high attenuation of periodic disturbances was achieved with the state feedback controller. The sensorless control system also exhibited a high performance rate during the start-up operation of the machine actual speed, while the estimated speed showed a longer duration in attaining a steady state with a good tracking of the actual speed. A robust start-up transient of the machine was also achieved with good tracking between the actual developed torque and the estimated torque during a no-load and a full load condition. In summary, the outcome of this paper proved

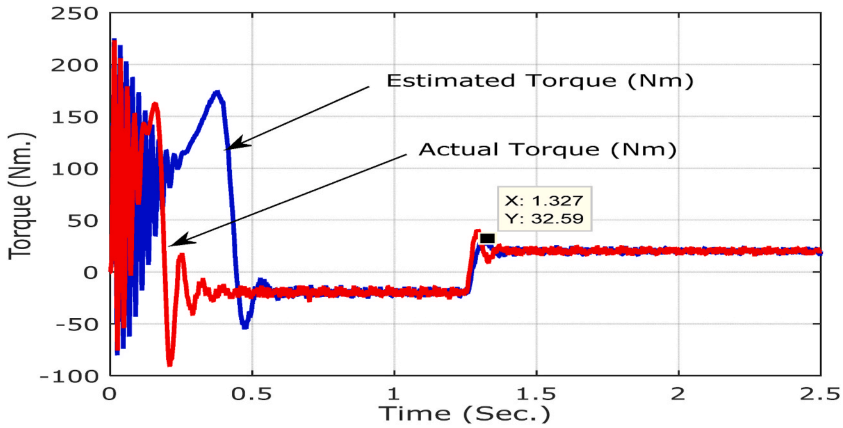

Fig. 19. Torque response to Load Changes for a Sensorless PMSM Drive Control.

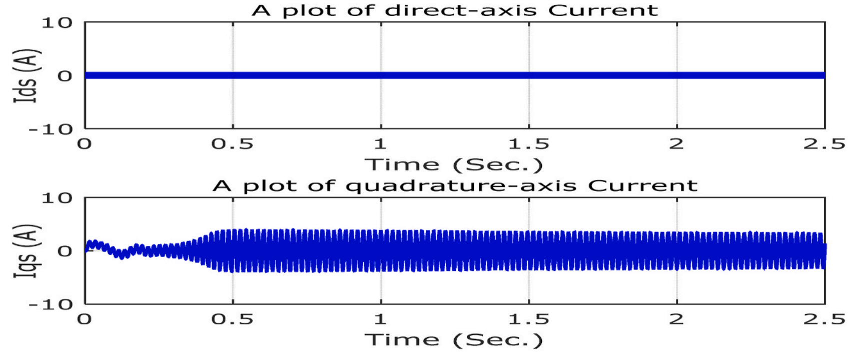

Fig. 20. dq-axes current for a Sensorless PMSM Drive Control.

that SFC controller with a proper parameter selection gave a robust control with good transition time than the traditional PID Controller while a Sensorless speed control offered an excellent drive performance with the attainment of steady state at a faster rate during a full load condition which reduces the risk of machine downtime and overheating effects.

5.2. Recommendations

For an effective control and drive performance of a permanent magnet synchronous machine with reduced periodic disturbances, a state feedback controller with linear quadratic regulator was adopted and recommended in this paper over the conventional PID-controller. The real-life implementation of the simulated work was an obvious limitation due to dearth of laboratory equipment and the needed facilities for validation. The scope for future work therefore is on how to experimentally validate the simulation results to conform to the standard best practice and also serve as a justification of the research work.

Declarations

Funding: Authors declare no funding for this research.

CRediT authorship contribution statement

Crescent Onyebuchi Omeje: Writing – original draft, Visualization, Software, Methodology, Formal analysis, Conceptualization. **Ayodeji Olalekan Salau:** Writing – review & editing, Visualization, Validation, Methodology, Investigation, Data curation. **Candidus Ugwoke Eya:** Software, Investigation.

Declaration of competing interest

The authors declare that they have no known competing financial interests or personal relationships that could have appeared to influence the work reported in this paper.

Acknowledgements

Not applicable.

References

[1] J. Liu, H. Li, Y. Deng, Torque ripple minimization of PMSM based on robust LC via adaptive sliding mode control, IEEE Trans. Power Electron. 33 (No. 4) (2017) 3655–3671, https://doi.org/10.1109/tpel.2017.2711098.
[2] B. Yi, S.N. Vukosavić, R. Ortega, A.M. Stanković, W. Zhang, A new signal injection-based method for estimation of position in interior permanent magnet synchronous motors, IET Power Electron. 13 (No. 9) (2020) 1865–1874, https://doi.org/10.1049/iet-pel.2019.1558.
[3] S. Luo, X. Chen, Y. Song, C. Guo, H. Shu, Design of model predictive controllers for PMSM drive system based on the extended kalman filter observer, Ijehv 11 (No. 4) (2019) 378–394, https://doi.org/10.1504/ijehv.2019.10024319.
[4] A.T. Nguyen, M.S. Rafaq, H.H. Choi, J.-W. Jung, A model reference adaptive control based speed controller for a surface-mounted permanent magnet synchronous motor drive, IEEE Trans. Ind. Electron. 65 (No. 12) (2018) 9399–9409, https://doi.org/10.1109/tie.2018.2826480.
[5] Y. Zhan, J. Guan, Y. Zhao, An adaptive second-order sliding-mode observer for permanent magnet synchronous motor with an improved phase locked loop structure considering speed reverse, Trans. Inst. Meas. Control 42 (No. 5) (2020) 1008–1021, https://doi.org/10.1177/0142331219880712.
[6] W.H. Chen, J. Yang, L. Guo, S. Li, Disturbance-observer based control and related methods- an overview, IEEE Trans. Ind. Electron. 63 (No. 2) (2016) 1083–1095, https://doi.org/10.1109/tie.2015.2478397.
[7] X. Sun, M. Wu, Z. Yang, G. Lei, Y. Guo, High-performance Control for a Permanent-Magnet Linear Synchronous Generator Using State Feedback Control Scheme Plus Grey Wolf Optimization, IET Electric Power Applications, 2020, pp. 1–10, https://doi.org/10.1049/iet-epa.2019.0383.
[8] J. Yang, W. Chen, S. Li, L. Guo, Y. Yan, Disturbance/uncertainty estimation and attenuation techniques in PMSM drives—a survey, IEEE Trans. Ind. Electron. 64 (No. 4) (2017) 3273–3285, https://doi.org/10.1109/tie.2016.2583412.

[9] Q. Zhu, Stabilization of stochastic non-linear delay systems with exogenous disturbances and the event-triggered feedback control, IEEE Trans. Automat. Control 64 (No. 9) (2019) 3764–3771, https://doi.org/10.1109/tac.2018.2882067.

[10] Q. Zhu, H. Wang, Output feedback stabilization of stochastic feed-forward systems with unknown control coefficients and unknown output function, Automatica 87 (2018) 166–175, https://doi.org/10.1016/j.automatica.2017.10.004.

[11] S. Singh, A.N. Tiwari, "Various Techniques of Sensorless Speed Control of PMSM: A Survey," Second International Conference on Electrical, Computer and Communication Technologies (ICECCT), 2017, pp. 1–6, https://doi.org/10.1109/icecct.2017.8117995. Coimbatore.

[12] L. Xiaoquan, L. Heyian, H. Junlin, Load disturbance observer-based control method for Sensorless PMSM drive, IET Electr. Power Appl. 10 (No. 8) (2016) 735–743, https://doi.org/10.1049/iet-epa.2015.0550.

[13] G. Zhenjie, B. Xin, Z. Chengning, G. Youguang, Robust sliding mode control of the permanent magnet synchronous motor with an improved power reaching law, Energies 15 (No. 5) (2022) 19–35, https://doi.org/10.3390/en15051935.

[14] Shihua Li, Huixian Liu, Wenshu Fu "An improved predictive functional control method with application to PMSM systems,", Int. J. Electron. 104 (No.1) (2017) 126–142, https://doi.org/10.1080/00207217.2016.1196743.

[15] T. Tarczewski, L.M. Grzesiak, "Constrained state feedback speed control of PMSM based on model predictive approach,", IEEE Trans. Ind. Electron. 63 (No. 6) (2016) 3867–3875, https://doi.org/10.1109/tie.2015.2497302.

[16] Abir H., Yemna B., Seifeddine B., Elghali M., and Naceur A. "Sliding mode observer based sensorless control of five phase PMSM in electric vehicle," 24-26 March 2019 19th International Conference on Sciences and Techniques of Automatic Control and Computer Engineering (STA), pp. 1867-4863. Sousse, Tunisia. DOI: 10.1109/sta.2019.8717290.

[17] Z. Qiao, T. Shi, Y. Tan, C. Xiu, X. He, New Sliding mode observer for position Sensorless control of permanent magnet synchronous motor, IEEE Trans. Ind. Electron. 60 (No. 2) (2013) 710–719, https://doi.org/10.1109/tie.2012.2206359.

[18] Yi Yang, Lubing Xu, Xiangxiang Fan, Disturbance observer-based L1 robust tracking control for hypersonic vehicles with T-S disturbance modeling 38 (No. 6) (2016) 742–750, https://doi.org/10.1177/1729881416671117.

[19] A. Apte, U. Thakar, V. Joshi, Disturbance observer based composite speed control of PMSM using fractional order PI-Controller, IEEE/CAA J. Autom. Sin. 6 (No.1) (2019) 316–326, https://doi.org/10.1109/jas.2019.1911354.

[20] Qiang Fei, Yongting Deng, Hongwen Li, Jing Liu, Meng Shao, Speed ripple minimization of permanent magnet synchronous motor based on model predictive and iterative learning controls, IEEE Access 7 (2019) 31791–31800, https://doi.org/10.1109/access.2019.2902888.

[21] Yaoqiang Wang, Yutao Feng, Xiaoguang Zhang, Jun Liang, A new reaching law for ant-disturbance sliding mode control of PMSM speed regulation system, IEEE Trans. Power Electron. 35 (2020) 4117–4126, https://doi.org/10.1109/tpel.2019.2933613.

[22] Yong-ting Deng, Jian-li Wang, Hong-wen Li, Da-peng Tian, Adaptive sliding mode current control with sliding mode disturbance observer for PMSM drives, ISA Trans. 88 (2019) 113–126, https://doi.org/10.1016/j.isatra.2018.11.039.

[23] Q. Song, C. Jia, Robust speed controller design for permanent magnet synchronous motor drives based on sliding mode control, Energy Proc. 88 (2016) 867–873, https://doi.org/10.1016/j.egypro.2016.06.102.

[24] X. Zhang, L. Sun, K. Zhao, L. Sun, Nonlinear speed control for PMSM system using sliding mode control and disturbance compensation techniques, IEEE Trans. Power Electron. 28 (2013) 1358–1365, https://doi.org/10.1109/tpel.2012.2206610.

[25] X. Liu, H. Yu, J. Yu, L. Zhao, Combined speed and current terminal sliding mode control with nonlinear disturbance observer for PMSM drive, IEEE Access 6 (2018) 29594–29601, https://doi.org/10.1109/access.2018.2840521.

[26] P. Gao, G. Zhang, H. Ouyang, L. Mei, A sliding mode control with nonlinear fractional order PID sliding surface for the speed operation of surface mounted PMSM drives based on an extended state observer, Math. Probl Eng. 18 (2019) 1–3, https://doi.org/10.1155/2019/7130232.

[27] L.M. Grzesiak, T. Tarczewski, PMSM servo drive control system with state feedback and load torque feed forward compensation, in: 15th International Power Electronics And Motion Control Conference, EPE-PEMC 2012 ECCE, Europe, Navi Sad, Serbia, 2012, https://doi.org/10.1108/03321641311293939.

[28] F. Mendoza-Mondragon, V.M. Hernandez-Guzman, J. Rodriguez-Resendiz, Robust speed control of permanent magnet synchronous motors using two degrees of freedom control, IEEE Trans. Ind. Electron. 65 (No. 8) (Aug. 2018) 6099–6108, https://doi.org/10.1109/tie.2017.2786203.

[29] C.O. Omeje, Dynamic analysis of a three phase 20hp, 400V, 50Hz induction machine driven by a hybrid voltage source inverter under a varying machine load, Int. J. Sci. Eng. Res. 9 (5) (2018) 2134–2150.

[30] W.J. Xu, Permanent magnet synchronous motors with linear quadratic speed controller, Energy Proc. 14 (2012) 364–369, https://doi.org/10.1016/j.egypro.2011.12.943.

[31] A.W. Yesgat, A.O. Salau, H.E. Kassahun, Fuzzy based sliding mode control of vector controlled multiphase induction motor drive under load fluctuation, J. Electr. Electron. Eng. 15 (No. 2) (2022) 98–105.

[32] A.S. Bosera, A.O. Salau, A.G. Yadessa, K.A. Jembere, Finite time trajectory tracking of a mobile robot using cascaded terminal sliding mode control under the presence of random Gaussian disturbance, in: Lecture Notes of the Institute for Computer Sciences, Social Informatics and Telecommunications Engineering, vol. 455, Springer, Cham, 2023, https://doi.org/10.1007/978-3-031-28725-1_5.

[33] A. Ashagrie, A.O. Salau, T. Weldcherkos, Modeling and Control of a 3-DOF articulated robotic manipulator using self-tuning fuzzy sliding mode controller, Cogent Eng. 8 (No. 1) (2021) 1950105, https://doi.org/10.1080/23311916.2021.1950105.

[34] A.O. Salau, K. Kanchana, K.J. Anoop, E.D. Markus, S.L. Braide, Suppression of over voltage in SiC-based inverter fed induction motor, Aust. J. Electr. Electron. Eng. (2023) 1–18, https://doi.org/10.1080/1448837X.2023.2250132.

[35] C.O. Omeje, A.O. Salau, Torque ripples enhancement of a PMBLDC motor propelled through quadratic DC-DC boost converter at varying load, ISA Transaction 143 (2023) 385–397, https://doi.org/10.1016/j.isatra.2023.08.027.

[36] Ł.J. Niewiara, R. Szczepanski, T. Tarczewski, L.M. Grzesiak, State feedback speed control with periodic disturbances attenuation for PMSM drive, Energies 2022 15 (587) (2022) 1–18, https://doi.org/10.3390/en15020587.